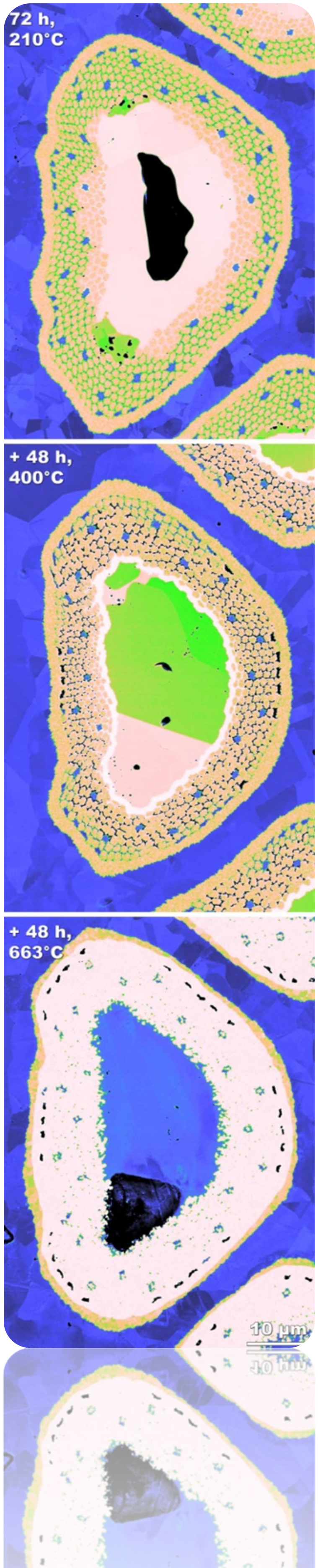

Final Scientific/Technical Report CY2011-4

DOE award number:
DE-FG02-07ER41451

Name of recipient:
Florida State University

Project title:
HIGH FIELD SUPERCONDUCTOR DEVELOPMENT
AND UNDERSTANDING

Lead Investigators:
David C. Larbalestier
Email: larbalestier@asc.magnet.fsu.edu
Tel: (850) 645-7483

Co-Principal Investigator:
Peter J. Lee
Email: lee@asc.magnet.fsu.edu
Tel: (850) 645-7484

Distribution limitation notices: None

Cover image: The critical journey of state-of-the-art RRP® conductor from distinct Sn, Nb and Cu components through an inhomogeneous first stage HT designed to solidify liquid Sn, through a more homogeneous all solid Sn-Cu phase mixture at 400 C through a hoped-for minimum inhomogeneity Nb_3Sn reaction. The phases present are made visible by false-colored atomic-number-sensitive-FESEM-back-scattered electron images of one of the new "Low-Sn" HEP RRP® Nb_3Sn strands (courtesy of the HEP-CDP) after the initial 72 h at 210 °C stage I heat treatment, then the 48 h at 400°C stage II HT and finally after the final 48 h at 663°C Nb_3Sn reaction heat treatment. The images show a sub-element from the outer corner for each stage. The distribution of Cu-Sn phases after the first stage is quite inhomogeneous as evidenced by the quite variable penetration of Sn into the Cu surrounding the filament pack. After stage II a uniform inner ring ("membrane") of ternary Cu-Nb-Sn phase (Nausite) is produced, separating the high-Sn core from the filament pack. This ring may be crucial to allowing a homogeneous Nb_3Sn reaction. Heat treatments were performed by Arup Ghosh at BNL as part of the LARP and CDP program.

Contents

I. EXECUTIVE (LAYMAN) SUMMARY

All present circular accelerators use superconducting magnets to bend and to focus the particle beams. The most powerful of these machines is the large hadron collider (LHC) at CERN. The main ring dipole magnets of the LHC are made from Nb-Ti but, as the machine is upgraded to higher luminosity, more powerful magnets made of Nb_3Sn will be required. Our work addresses how to make the Nb_3Sn conductors more effective and more suitable for use in the LHC.

The most important property of the superconducting conductor used for an accelerator magnet is that it must have very high critical current density, the property that allows the generation of high magnetic fields in small spaces. Nb_3Sn is the original high field superconductor, the material which was discovered in 1960 to allow a high current density in the field of about 9 T. For the high luminosity upgrade of the LHC, much higher current densities in fields of about 12 Tesla will be required. The critical value of the current density is of order 2600 A/mm^2 in a field of 12 Tesla. But there are very important secondary factors that complicate the attainment of this critical current density. The first is that the effective filament diameter must be no larger than about 40 µm. The second factor is that 50% of the cross-section of the Nb_3Sn conductor that is pure copper must be protected from any poisoning by any Sn leakage through the diffusion barrier that protects the package of niobium and tin from which the Nb_3Sn is formed by a high temperature reaction.

These three, somewhat conflicting requirements, mean that optimization of the conductor is complex. The work described in this contract report addresses these conflicting requirements. They show that very sophisticated characterizations can uncover the way to satisfy all 3 requirements and they also suggest that the ultimate optimization of Nb_3Sn is still not yet in sight.

II. COMPARISON OF THE ACTUAL ACCOMPLISHMENTS WITH THE GOALS AND OBJECTIVES OF THE PROJECT.

1. **Nb_3Sn**: Define the limits to high field performance of practical conductors of the generally non-stoichiometric, A15 compound Nb_3Sn by making detailed measurements of the distribution of A15 phase compositions in conductors and comparing such distributions to the property variations found in specially fabricated bulk, homogeneous A15 samples made with the Sn, Cu, Ti and Ta additions that are important in real conductors. We believe that this understanding will enable a summary evaluation of whether further efforts to push the boundaries of Nb_3Sn conductor properties are still effective or whether Nb_3Sn, like Nb-Ti in the 1990s, has reached its effective critical current density (J_c), upper critical field H_{c2} or irreversibility field H_{irr} limits. Actual accomplishment: This was the principal effort of our work during this three-year contract period, as will be described in the following sections.

2. **Cuprates**: High temperature superconductors like round wire (RW) Bi-2212 ($Bi_2Sr_2CaCu_2O_x$) and coated conductor (CC) tapes of $YBa_2Cu_3O_{7-\delta}$ (YBCO) will receive greater emphasis because magnet-useful conductors are now developing. We here describe a fundamental program to understand properties of single GBs of 2212, doped YBCO and Nb_3Sn because any breakout to the conductor that we really want requires GBs that can better transmit supercurrent. Because ongoing funding in 2012 and 2013 of the ARRA efforts on RW 2212 are uncertain, it is possible that some redirection of this effort towards nearer term conductor needs may be appropriate, but such a determination cannot be usefully made until late 2011. Actual accomplishments: in fact bridge support was supplied by DOE-HEP through Fermilab so we did not need to slow down our Nb_3Sn work to keep the very promising 2212 work alive before its independent funding started on July 1, 2013.

3. **Community Support**: We will continue to provide direct scientific support to the HEP community through continued collaborations with the National Laboratory magnet programs like the Conductor Development Program (CDP) that underpins LARP (Large Accelerator Research Program) and MAP (Muon Accelerator Program) and any ongoing broader collaborations such as

VHFSMC (Very High Field Superconducting Magnet Collaboration), applying our core expertise of microstructural and superconducting property measurements to the ongoing development of better HEP-relevant conductors. Actual accomplishments: we participated strongly in all of the above HEP programs, and also became the lead US laboratory contact for the CERN–led EUCARD2 program to develop HTS dipole magnets.

4. **Training**: We will continue to provide forefront training to undergraduates, graduates and post-doctorals, maintaining our stream of highly effective and leading personnel to the HEP and the Applied Superconductivity communities. Actual accomplishments: we graduated two PhD students during this period and one of them is now a postdoc at Fermilab, while 3 ongoing PhD students were supported. A partially supported postdoc transitioned to a position as Visiting Assistant Scientist at the NHMFL.

5. **Outreach**: We will continue to co-organize the Low Temperature/High Field Superconductor Workshop (LTSW/HFSW) and provide on-line resources such as the widely trusted master critical current density plot. We will remain active in the broader community through our memberships of various workshop and international conference committees (e.g. IEEE-CSC, ICMC, ASC'12, ISS, CCA). Actual accomplishments: we were lead organizers of the 2011, 2012 and 2013 LTSW/HFSW and played organizing roles in the 2012 and 2014 applied superconductivity conferences, as well as several other meetings. We became lead US partners in the EUCARD2 consortium organized from CERN.

Details of these accomplishments now follow.

III. SUMMARY OF PROJECT ACTIVITIES.

When this grant started in July 2011, there was still intense effort to develop the properties of the two leading contenders of HEP-relevant Nb_3Sn conductors made by the RRP® and the PIT processes. The driving question for our studies was: have the limits to performance of these two processes been achieved yet and can the highest values of critical current density demonstrated by these two processes at the filament sizes of the order 70 µm be obtained at smaller filament sizes half this size? Our work thus naturally organized itself into a series of sub-questions:

1. Within the package needed to produce the A15 phase, Nb_3Sn superconductor, how much A15 phase, how much residual diffusion barrier, and how much residual core from which the tin was supplied remains and how different are these proportions between PIT and RRP®? A very important outcome from posing this question is that we found that there is an almost 50% advantage in the amount of useful A15 phase formed from the Sn, Nb and Cu package for RRP compared to PIT.

2. Because the A15 phase field of Nb_3Sn has a significant compositional and superconducting property variation, we wanted to develop a method by which we could measure this variation and correlate it directly to transport critical current measurements. Although not easy, we have found that measurements of the specific heat in 0 T and in 16 T provide such information.

3. It was believed at the outset of this grant that the reaction paths to the A15 phase were fundamentally different in RRP and in PIT conductors. An open question was whether the grain boundaries (GBs) that provide the vortex pinning had similar compositions. We therefore wanted to make quantitative measurements of the grain boundary density in the A15 phase so that we could measure the fundamental flux pinning force Q_{GB} exerted by the grain boundaries in both PIT and RRP conductors. In fact we found that Q_{GB} was very similar between the 2 phases, provided that we included only the fine grain A15 component of the PIT material. This prompted study of (i) the nature of chemical segregants to the GB

and indeed we found Cu segregated to both RRP and PIT GBs, a result that then led us (ii) to consider the reaction path of PIT. Confirming an earlier XRD study of Scheuerlein, we found that the carefully made $NbSn_2$ powder that distinguishes the PIT from the RRP route reacts above about 300 °C to form the same Cu-Sn-Nb Nausite phase that is in the RRP reaction path. Comparing the quantities of A15 with their effective GB pinning strength thus allows us to discriminate the effect of the quantity of A15 phase (in RRP favor) from its quality (similar).

4. An effective diffusion barrier is needed to protect the stabilizing copper which is essential to reliable magnet performance. These diffusion barriers become less effective at smaller effective filament diameters, especially in regions which are heavily deformed along the narrow edge of the Rutherford cable. We therefore have done comparative assessments of the deformation of these barriers to understand again if there is any fundamental difference between PIT and RRP conductors. We also were able to establish that RRR degradation below 100 occurs for <5% barrier breaks for both PIT and RRP, making a detailed understanding of the effect of deformation on barrier quality quite vital.

5. Throughout this whole period we have remained very open to collaborations with other groups, especially where our unique capabilities could be helpful in answering questions driven by other principal investigators. In this way we have been able to tackle the origin of a very surprising dependence of the magnitude of the irreversible strain in tension on the nature of the alloying elements in Nb_3Sn driven by Najib Cheggour at NIST. As noted in our cover page image, we have worked very closely with Arup Ghosh at Brookhaven, who kept us closely coupled to the work being performed by the LARP collaboration. We also benefited from a close collaboration with Amalia Ballarino who supplied us numerous PIT samples from the latest Bruker procurements.

We now present more detailed answers to these driving questions of our work.

III-1 NB_3SN

III-1A. RRP: MICROCHEMICAL PROPERTIES (PETER LEE AND CHARLIE SANABRIA)

The microchemical analysis performed on RRP revealed compositional gradient at multiple levels. Not only Sn gradients but also Ta gradients on the filament scale were found in Ta-doped RRP. These different Sn-distributions in the reacted A15 observed in Ta and Ti strands will be essential to the ongoing task of finding a root cause of the origin of their different irreversibility strain limit.

The microchemistry of PIT strands is relatively simple and well established [1, 2] with a shallow uniform Sn gradient radial from core across the A15 gradient; in RRP® strands, however, there are gradients across both the original filaments and radially across the whole sub-element and there may also be variations in the distributions of the Ti or Ta dopants. In our previous reports

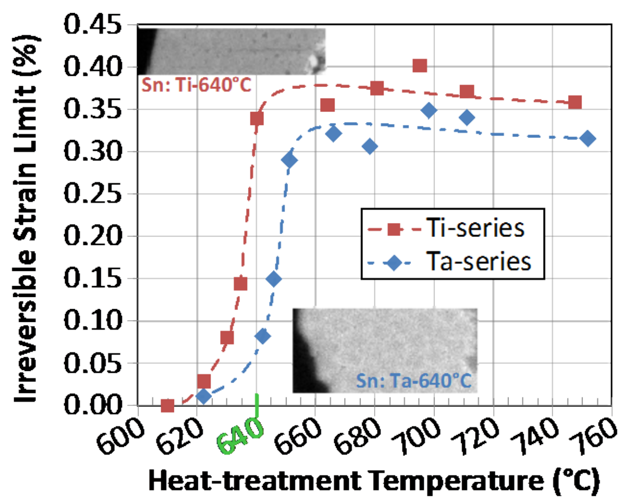

Figure 1. Sensitivity of irreversibility strain for 54/61 RRP® strand to heat treatment temperature for Ti and Ta doped strands as measured by Najib Cheggour and coworkers at NIST-Boulder (heat treatments at BNL and FSU). Inset we show EDS maps for Sn (L line) across the A15 layers in Ta and Ti and strands heat treated at 640°C for 48 hr. There is a much more inhomogeneous distribution of Sn in the Ta-doped strand.

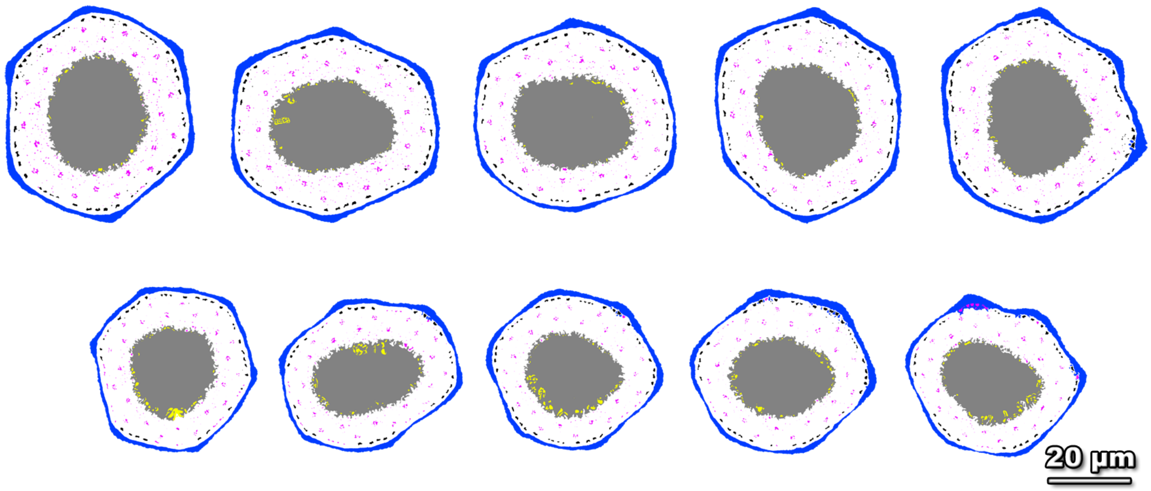

Figure 2. Five sub-elements of a 0.85 mm strand (top) and five sub-elements of a 0.7 mm strand showing a detailed study of the positional variation of diffusion barrier thickness. One issue emerging from the techniques being applied to the latest RRP billets is that it is possible to draw down to smaller size without getting barrier breakdown. Small areas of yellow-tinted ternary Cu-Nb-Sn Nausite phase have been seen in some conductors and their presence will be tracked through

we showed that there are local concentrations of Ti dopant at the grain boundaries, and that Ti may also be inhomogeneously distributed on the macro-scale, as shown by our EDS mapping. Perhaps even more surprisingly we saw filament scale gradients in not only Sn but also Ta in Nb-Ta rod processed RRP® strand and this work (in collaboration with Arup Ghosh at Brookhaven) has recently been published [5]. Our current collaboration with BNL is an examination of the new lower Sn RRP designs that are showing greater RRR resilience after reaction with only minor loss of J_c. This is prompting a reevaluation of the heat treatment process to see if the J_c can be recovered. In the cover images we show the remarkable changes that occur in the RRP® strand cross-section during the initial heat treatment steps, particularly as a Cu-Sn-Nb Nausite "membrane" forms at the Sn core/filament pack interface. The behavior of the "membrane" is of particular interest now that there are signs that a similar membrane may be beneficially impacting some filaments in PIT strands too as shown in a following section. We should not forget here the valuable study of Pong *et al* who recently highlighted the important role of a membrane in controlling the development of high J_c in RRP strands of varying Cu:Sn ratio [3]. In work being carried out by Sanabria in collaboration with OST, this reaction feature is going to receive detailed attention.

Another major collaboration has been with Najib Cheggour and co-workers at NIST-Boulder/Univ. of Colorado, who have been studying the irreversibility tensile strain of Nb_3Sn composites. We have been providing the microstructural and microchemical analysis of the strands, as well as picking up the heat treatments when BNL was no longer able to continue due to staffing cuts. The remarkable results of this study first presented at the Applied Superconductivity Conference, in Charlotte NC in August 2014 are summarized in Figure 1. Both Ta and Ti doped RRP® strands undergo a very sharp transition in their irreversibility behavior with heat treatment temperature, with the reduced irreversibility strain starting below 640°C for Ti and 650°C for Ta. The cause is as yet unknown but our microchemical analysis shows that the Sn distribution in the Ti strand is much more homogenous (see inset EDS maps). The ARRA funded fast-EDS SDD detector has been particularly helpful for this project. Exploration of root cause is ongoing in our new grant.

To address the full potential of the RRP strand we opened discussions with OST to see if a much closer collaboration and quantification of the RRP conductor would be possible. This offer was enthusiastically taken up by OST and it became clear that the best way to enable us collaboration was by arranging for one of our PhD students to spend part of his time at OST interacting strongly with the OST staff, doing as much work as he could at OST and then bringing problems that could only be resolved at ASC back to Tallahassee. The student that we selected, Carlos (Charlie) Sanabria had previously worked extremely closely with ITER on the deconstruction of the ITER cable [4]. Sanabria has been working closely with OST since early 2014, with the aim of rapidly improving the quantification of RRP wires using digital microscopy and metallography at both the OST manufacturing facility in Carteret NJ as well as at FSU. Currently both J_c and RRR degrade as the sub-element size is reduced. These smaller sub-element sizes also produce scattered properties and it is not clear if this scatter is a result of production scatter or if there is something fundamentally different occurring during the reaction of smaller sub-elements.

Initial characterization of two representative strands at different sizes (0.85 mm and 0.7 mm) has revealed that the smaller sub-elements tend to have more Nb dissolution into the core with formation of the ternary Nausite phase identified by the yellow features in Figure 2. These smaller strands also show more unreacted filaments close to the barrier, thus indicating a loss in the amount of A15 phase that can be formed. This is the first indication that there is something fundamentally different in the reaction of these smaller sub-elements. Reverting to the images which are shown on the front cover of this report, we are concerned that immediately after the 2nd heat treatment at 400°C, the conductor again enters a zone where there is extensive liquid present and where the initial stages of the Nb_3Sn reaction may occur quite inhomogeneously. We anticipate paying much more attention to this 3rd phase of the heat treatment in our ongoing work. The key point is that degraded critical current density is not primarily due to loss of Sn through a bad diffusion barrier. It seems to be that there is a change in the reaction conditions that make the Nb_3Sn.

III-1B. RRP: Superconducting Property Homogeneity evaluations by Specific Heat (Chiara Tarantini)

We believe that our specific heat investigations are by far the most comprehensive yet undertaken on Nb_3Sn. We have had to invest considerable time in preparing our 16 T PPMS instrument to make it suitable for this investigation but we now believe that it is a vital and very important tool for understanding the degree of inhomogeneity which exists in all high performance Nb_3Sn strands. As we make a study of many recent conductors, we are picking up many unexpected variations of homogeneity that we believe are essential to understand if Nb_3Sn is to be finally optimized.

A first investigation was of whether there were significant differences depending on whether the H_{c2}-enhancing dopant was Ti or Ta. We investigated RRP strands prepared with different dopants, with normal and with the new reduced Sn content (and higher RRR) strands. We found that though the reduced Sn content strand does produce less A15 in the cross-section, it does not worsen the homogeneity of the A15 phase and it does not modify its intrinsic properties. By contrast, the A15 homogeneity is more strongly affected by the type of doping element: Ti-doping produces a significantly more homogeneous A15 than does Ta-doping, thus positively improving also the in-field performance.

To ensure the reliability of our comparison, we characterized three different 108/127 strands with the same design that were similarly heat treated.

Table 1 RRP strand characteristics (design, Sn content and doping), heat treatment performed and strand properties (non-Cu J_c(12T) and Kramer field).

	RRP14895	RRP14896	RRP12879
Design	108/127, 0.778mm diam.	108/127, 0.778mm diam.	108/127, 0.778mm diam.
Sn content	Standard Sn	5% less Sn	Standard Sn
Doping	Ti	Ti	Ta
Heat Treatment	662°C/48h	662°C/48h	665°C/48h
J_c(12T), A/mm^2	**3035**	**2927**	**2950**
$\mu_0 H_k$, T	25.45	25.47	23.84

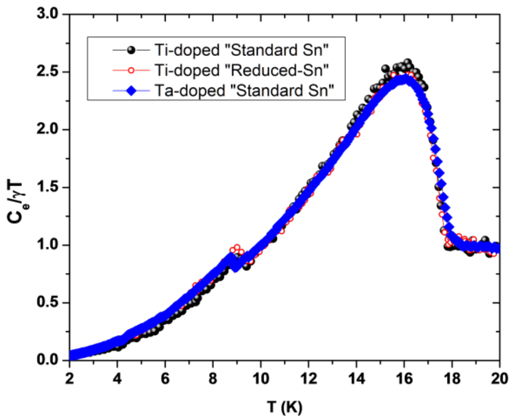

Figure 3. Normalized electronic specific heat for the 3 studied RRP strands.

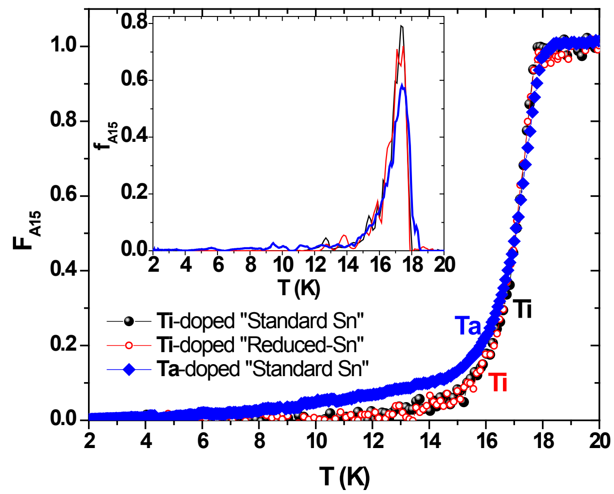

Figure 4 Zero-field T_c-distribution of the A15 phase (f_{A15}, inset) and its integral (F_{A15}, main panel) in three differently doped RRP strands. The Ti-doped strands have markedly sharper T_c distributions.

The original purpose of reducing Sn was to reduce Nb barrier breakage so as to maintain a high Cu RRR, whereas changing doping affects the in-field performance. Here we compare strands heat treated at 662-665˚C for 48 h. Two of them are Ti-doped, but with different Sn contents: one strand is made with standard Sn (RRP14895), one with 5% less Sn (RRP14896). The third strand is a Ta-ternary strand with standard Sn (RRP12879). The main properties of these strands are summarized in Table 1. The first practically important observation is that reducing the Sn content in the Ti-doped strands has only a small J_c effect, only 3-4% of J_c being lost, and also without effect on the irreversibility field ($\mu_0 H_k$). Rather surprisingly, although Ta-doping maintains J_c in the same range, it significantly reduced $\mu_0 H_k$ from ~25.5 T to ~23.8 T.

The specific heat characterization (Figure 3) shows that there is a difference in the T_c-onset between Ti and Ta doping: ~17.9 K for Ti strands and ~ 18.4 K for the Ta. Because of the different Sn content the reduced-Sn strand has a significant larger amount of residual unreacted Nb, 13.3%, compared to the standard Sn strands, 7.4-7.7% (estimated by the Sommerfeld constant ratio, not a volumetric estimation), thus showing that there is indeed less attack on the diffusion barrier. Despite the different Sn contents, the T_c-distribution of the A15 phase, f_{A15}, and its integral, F_{A15}, reveal that there is no significant difference between the A15 homogeneity in the two Ti-doped strands (see Figure 4), producing the good result that the main effect of the reduced Sn is simply to reduce the total amount of A15 without affecting its property distribution. Beneficially, most of this reduced A15 occurs by avoiding reaction of the diffusion barrier. On the other hand F_{A15} shows that Ta-doping produces a less homogenous A15 phase, despite its higher T_c-onset. This is particular evident comparing the low temperature behavior: the Ta-doped strand has a superconducting phase with T_c as low as 5-6 K, the lowest T_c obtainable for Sn-poor A15 phase, whereas both Ti-doped strands have no A15 phase with T_c lower than ~12 K. Considering their very similar billet designs and heat treatment, this finding indicates either that Ti induces a better diffusion of Sn in the A15 phase, decreasing the compositional gradient, or itself substitutes into the A15 lattice, modifying the low-Sn side of the A15 phase field. Comparing these results with our previous study on a 54/61 Ta-doped strand [5], we found that a comparably flat T_c-distribution at low temperature required heat treatment at a temperature as high as 750 °C, a temperature unsuitable for practical applications because of the heavy RRR degradation occurring at this temperature [5].

A similar analysis (Figure 5) of the 16 T specific heat characterizations shows almost identical T_c-distributions in the two Ti-doped strands, independent of their Sn content, but a significantly degraded one for the Ta-doped conductor. In fact this sample has a lower onset and a smaller amount of material still in superconducting state at 16 T [estimated as 1- F_{A15}(16 T)]: at 2 K and 16 T the Ti-doped strands still have 50-51% of the phase still is superconducting state, whereas the Ta-doped has only 42%. This indicates that Ti-doped A15 has better in-field performance for this heat treatment. This is an important validation of what was originally thought to be a step back in performance by forsaking Ta-doped Nb_3Sn for Ti-doped Nb_3Sn. In fact the Ti-doped conductors are cheaper to make and have better properties too, even at very high fields.

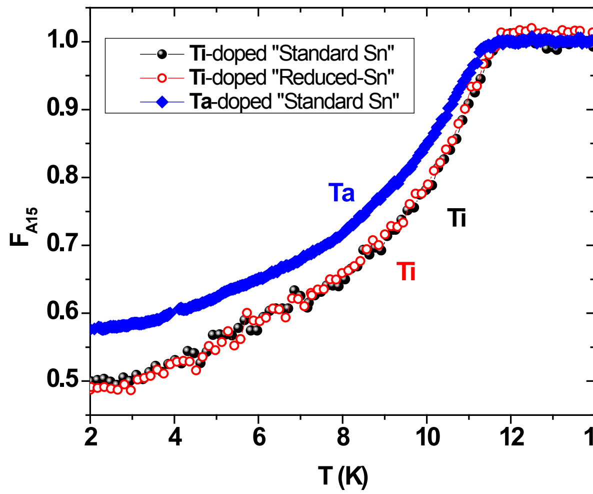

Figure 5. F_{A15}, integral of the A15 T_c-distribution at 16 T for the 3 studied RRP strands.

Although the full implications of these studies are not yet clear, the specific heat characterizations do show that there are significant differences from composite to composite and that they can be elucidated by measurements of the specific heat. These studies are therefore an essential component of the characterizations that are going to be carried out with OST on evaluating the reasons for the variability of the most recent composites that they are making for LARP and for the HiLumi project.

III-1c. PIT & RRP Deformation Studies (Graduate R.A. Michael Brown)

As noted earlier, the critical problem that limits the magnet performance of both RRP and PIT strands is the degradation of the diffusion barrier and consequent loss of RRR in conductors damaged during Rutherford cable manufacture (and occasionally due to mistakes in round wire drawing). Deformation studies of both RRP and PIT strand were thus performed to determine the effect on the sub-element shape, their diffusion barriers (DBs) and their consequent effect on the RRR of the Cu-stabilizer. The deformation studies of both RRP and PIT strand were thus performed to determine the effect on the sub-element shape and the consequent effect on the Cu-stabilized RRR. Interestingly, while round wire drawing preferentially damages the *outer* filaments or sub-bundles, non-round deformation by rolling or

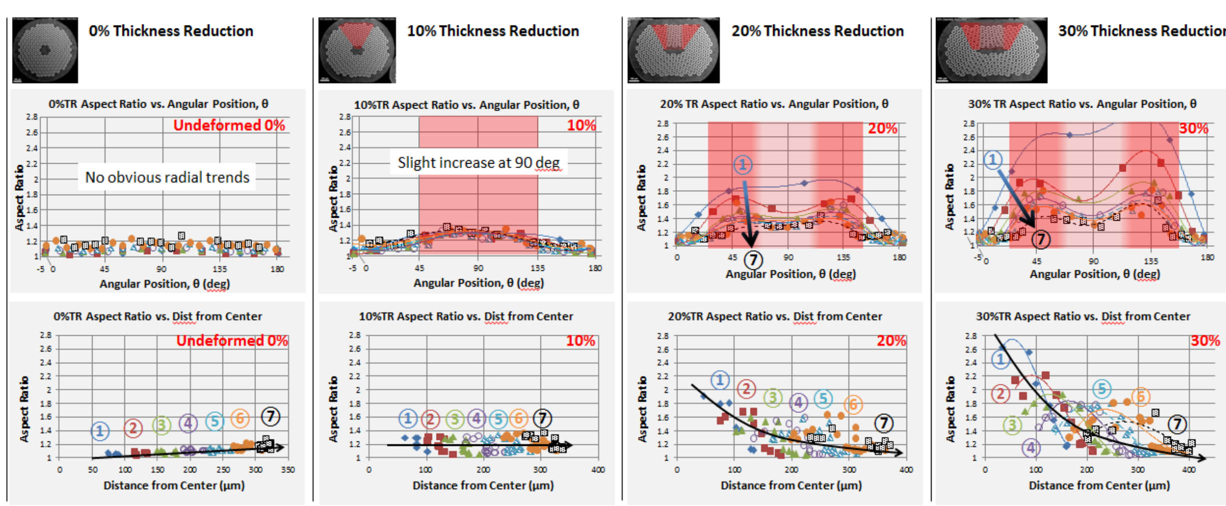

Figure 6. Strand cross sections are shown with graphical representation of filament distortion characteristics. Aspect ratio of each filament in the top half of the cross section is displayed and grouped in rings, numbered 1 through 6 going from inner rings to outer rings.

cabling preferentially damages the *inner* elements of the conductor. As a consequence the strand RRR tends to linearly decrease with increasing deformation.

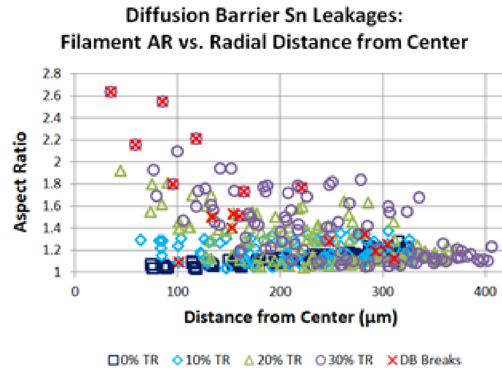

Figure 7. Distribution of filament diffusion barrier failures (DB Breaks). Data points indicate aspect ratio and distance from the center of the strand for each filament. Red “x” markers overlay data to show which filaments have been compromised by broken diffusion barriers and Sn leakage.

We have previously shown using digital analysis techniques that RRR degradation in the stabilizing Cu occurs when filaments become more oval in samples of Bruker PIT strand provided by Ballarino at CERN. Further experiments have been performed to more precisely connect the distortion of strand filaments to RRR degradation by subjecting the strand to varying degrees of rolling deformation before heat treatment, digitally characterizing the cross-section sub-element shapes, quantifying diffusion barrier failures, and measuring RRR.

Figure 6 presents the aspect ratio of the filament (a measure of its distortion) with respect to both its angular position within the strand and the distance of the filament or sub-element from the center of the strand (thus picking up the tendency of damage to locate preferentially to the strand center). Each matching set of data points represents a ring of filaments within the strand. The data show strong and increasing shear at 45˚ from the axis of deformation, as well as a prevalence for the inner filaments to deform more than the outer filaments upon increasing deformation. Quantification of filament diffusion barrier failure has been performed (Figure 7), correlating filament distortion with a higher prevalence of Sn leakage into the stabilizing Cu matrix. Note that 4 of the 5 diffusion barrier breaks occur for aspect ratios greater than 2.

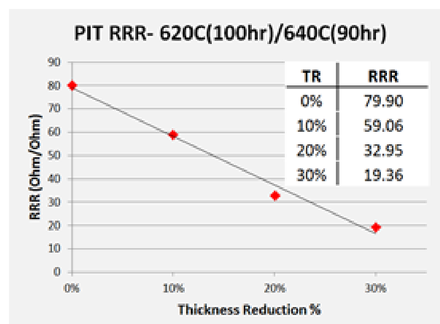

Figure 8. RRR values for varying amounts of strand deformation. Shows clear indication of RRR degradation as filaments become more highly

Figure 8 displays the values of RRR with respect to increasing thickness reduction of the strand, showing clear evidence of increased Sn leakage.

III-1D. PIT CONDUCTORS: RESULT SUMMARY

Three clear findings were determined by the study of PIT strands in these 3 years:

I. Coupled specific heat and magnetization analysis supported by microstructural characterization strongly support a conclusion that the large grain layer in PIT is not able to carry significant current (details ahead). This means that the only useful A15 is the small grain Nb_3Sn layer, about 40% of the non-Cu cross-section, as compared to about 60% of the RRP conductors (see next).

II. The starting sub-element constituents in PIT ($NbSn_2$, Cu and perhaps Sn) are very different from those in RRP strands (Nb, Cu and Sn). In fact, in order to maintain an acceptable RRR of the Cu-stabilizer, the PIT strand has to be heat treated in the 620-640 °C range leaving ~23% of residual Nb in the non-Cu cross section; in strong contrast, the residual Nb in RRP of equivalent filament diameter is <10%, even though more flexible heat treatments are employed. While the total A15 content occupies about 54-55% of the non-Cu cross-section in PIT, only ¾ of this is made up of useful small grains, while in RRP the A15 fraction is about 61-63% and substantially all of it is made of small grain (details are in Table 2).

III. In spite of this unpromising comparison between PIT and RRP, a possible break-through to improve the performance of PIT strand comes from analytical microscopy on the most recent 0.788 mm diameter PIT wire supplied by CERN to the US as part of the RRP for PIT exchange. It was found that some sub-elements have an atypical structure that produces 46% of small grain A15 with respect to 41% in the typical ones. Chemical analysis suggests the presence in these sub-elements of a regulating barrier (that membrane again) that controls Sn diffusion from the core into the Nb-Ta filament (details ahead).

Table 2 Comparison of 0.7mm-54/61 RRP and 1 mm-192stack PIT after heat treatments performed to maintain an acceptable RRR>100. Percentages are referred to the non-Cu cross-section.

	RRP	PIT
Effective filament d_{eff}	70 μm	50 μm
HT	650-680° C	625° C and 620+640° C
Diffusion barrier %	4%	23%
Total A15 %	61-63%	54-55%
Small grain A15 %	**61-63%**	**~41%**

III-1E. PIT: Identification of the Carrying-Current A15 (Chiara Tarantini and PhD Graduate Student Chris Segal)

In order to identify the portion of the strand carrying current we combined FESEM characterization, magnetization and specific heat measurements in the characterization of 1 mm-PIT wires being supplied for the FRESCA-2 magnet. Multiple FESEM-BSE images were used to define the average radial positions of the interfaces between core, large grain A15 (LG-A15), small equiaxed grain A15 (SeG-A15), small columnar grain A15 (ScG-A15), Nb barrier (Nb) and Cu stabilizer (Cu) as is schematically shown in the inset of Figure 9. Magnetization measurement revealed the Nb T_c transition, a double T_c transition for the A15 phase and a maximum T_c onset distinctly lower than that obtained in the specific heat measurement. A key advantage of contrasting magnetization and specific heat evaluations if that the first contains location information due to the shielding effect of the magnetic field while no location information is present in the specific heat. A simple model considers that the shielded volume in the magnetization experiment is temperature dependent due to the radial variation of T_c across each filament, allowing the shielded radius at any temperature to be estimated by the following equation:

$$r_{Shielded}(T) = 2 \times \sqrt{m/Hl}$$

where m is the magnetic moment, H the applied field and l the sample length. This allows direct comparison of the microstructural image of the conductor and the magnetization characterization, making it possible to identify the critical temperature corresponding to each interface (Figure 9, main panel). Here the positions of the Nb barrier/Cu stabilizer interface and small columnar grain/Nb barrier interface do correspond

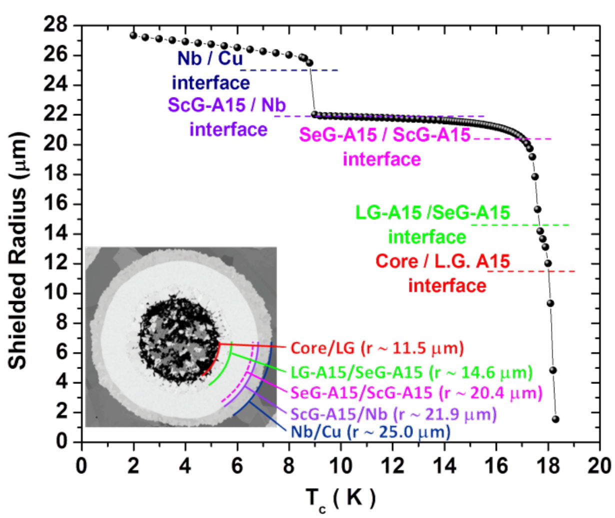

Figure 9 Shielded radius versus T_c as deduced by magnetization measurements superimposed with the radial position of the different layer interfaces as determined by FESEM-BSE image analysis (the reported value are averaged on several filaments.

to the beginning and end of the Nb transition, demonstrating the accuracy of the model. In this way the T_c values corresponding to the core/large A15 grain, large A15 grain/small A15 equiaxed grain and small equiaxed A15 grain/columnar A15 grain interfaces can all be determined and these three T_c values can then be compared to the T_c-distribution determined by specific heat which, unlike the magnetization measurement, has no positional information associated with it (Figure 11).

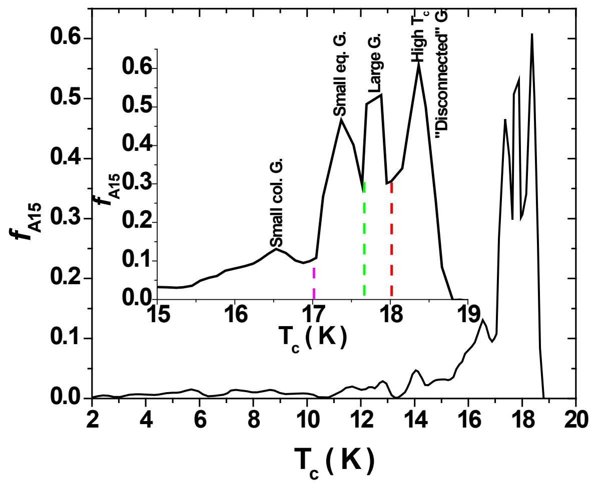

Figure 11 T_c distribution obtained by specific heat with indication of the T_c corresponding to the interfaces deduced from the correlation of magnetization and microstructure presented in Figure 9.

The specific heat T_c-distribution of the A15 phase reveals three major peaks above 17 K and a broadened distribution at lower temperature. Since the three T_c values determined by the magnetization shielding analysis fall at the minima between the peaks (vertical lines in the inset of Figure 11), we can relate the main peaks in the T_c-distribution to the different A15 morphologies present in the strand. The highest temperature peak in the specific heat T_c-distribution (Figure 11) is thus determined by disconnected grains in the core or by a few sparse high-T_c large grains that are incapable of generating a continuous percolative path. We believe that, being formed by reaction from the original $NbSn_2$ powder without Ta doping, they have a high T_c. The second peak in the specific heat T_c-distribution (at ~17.8-17.9 K) is generated by the majority of the large grains where we believe reaction involved also the Nb-Ta filament. Only the third peak, between 17 K and 17.7 K, is constituted of small equiaxed grains, whereas the low temperature tail below 17 K is determined by small columnar grains that form close to the Nb barrier.

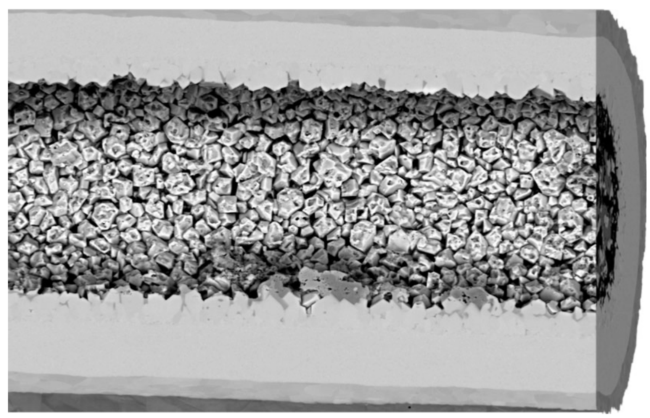
Figure 10 FESEM BSE image of a longitudinal cross section of a single filament from a Bruker PIT strand showing the large grain interior layer that is poorly connected.

Our striking conclusion here is that none of the A15 phase above 17.7 K can be associated with the small grain/high pinning A15 required for high J_c. Thus we conclude that the J_c of the PIT conductor must be ascribed to the fine grain region which forms only about ¾ of the total A15 in the geometrical cross-section. The poor connectivity of the large grain component formed at the core-A15 interface is also supported by the longitudinal cross-sectional image of a typical sub-element shown in Figure 10. Here half of the cylindrical filament has been polished away permitting a view of the core-A15 interface. The dark interface around each A15 grain is clear. Higher magnification images show that this is predominantly the Sn-rich Cu phase η.

III-1F. PIT: MACROSCOPIC PROPERTIES AND RRR (GRADUATE STUDENT CHRIS SEGAL)

Because ~25% of the A15 layer is made up of large, poorly connected grains that do not contribute significantly to J_c, reducing this non-contributing component could greatly improve PIT

Table 3. Compositions of two types of filament found in PIT conductors showing the advantage of the atypical ones.

	Typical	Atypical	
Element	At.%	At.%	%change
Nb	22.6	18.2	-20
SG A15	41.4	46.3	+12
LG A15	13.6	10.2	-25
Core	22.4	25.3	+13

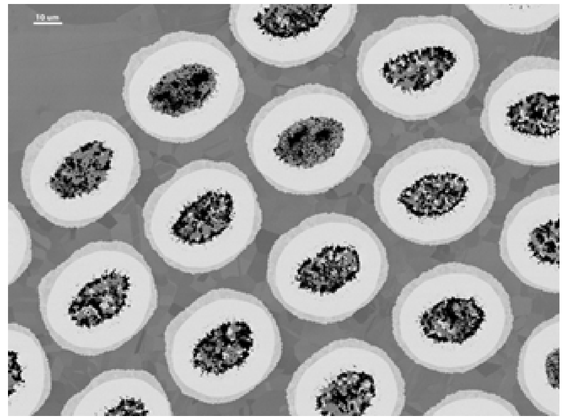

Figure 12 FESEM-BSE image of a polished transverse cross-section of a Bruker PIT strand heat treated at 630˚C for 240 h.

conductor performance. Recently we found two distinctly different filament types within a high performance PIT wire, one of which has a much lower large-grain (LG) quantity and an increased small grain (SG) component. Our examination of these filaments suggests the possibility of enhancing PIT strand performance.

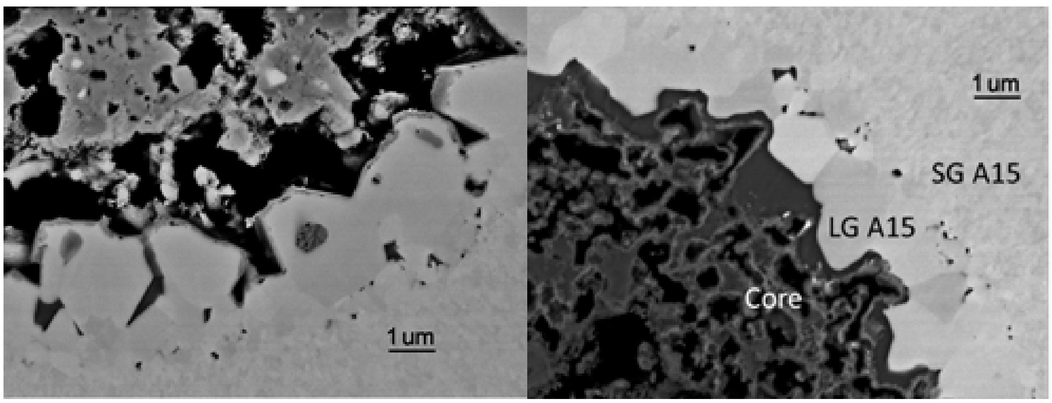

Figure 13. Left, atypical filament, right, is an atypical one whose core has little or no Sn left.

Figure 12 shows that some cores are darker than the others because they contain little residual Sn, implying that it is better utilized during the A15 reaction. In the magnified images of Figure 13 we see two distinct filament types after a CERN-optimized reaction at 630˚C for 240 h.

The atypical filaments produce a dramatically different ratio of final phases which are shown in Figure 14 and summarized in Table 3 (eight filaments of each type were averaged and the percentage change in the atypical, better filaments are included in the last column). To be specially noted is the 12% enhancement of small-grain and 25% reduction in large grain A15. We believe that this difference is caused by a membrane that regulates Sn diffusion into the filament. In the atypical filaments there is a Cu-rich layer that surrounds the LG (Figure 15) that forces constrains Sn diffusion into the Nb. We speculate that when there is too much Sn present then the A15 forms by a Sn-rich route that produces LG A15 by the $NbSn_2 \rightarrow Nb_6Sn_5 \rightarrow Nb_3Sn$ reaction route. But if there is a Cu- or Nb- rich membrane the reaction front has a lower Sn content layer which prevents the formation of

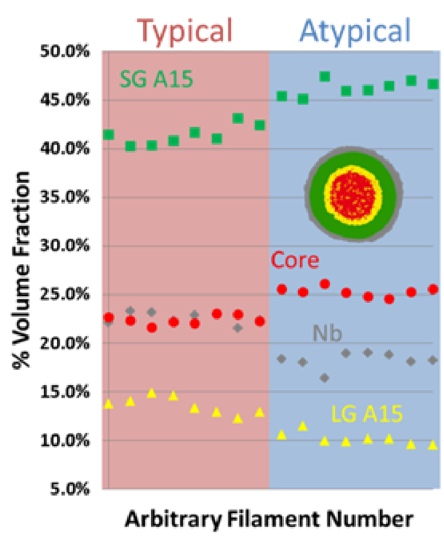

Figure 14 Volume fraction of SG A15, LG A15, Nb barrier and core for 8 typical filament (left) and 8 atypical filaments (right) showing that the atypical one are able to produce more small grain A15.

LG A15. Our new focus is to study how this membrane helps to reduce the LG A15 in favor for the small grain.

III-1G PIT-1 MM: SUPERCONDUCTING PROPERTIES BY SPECIFIC HEAT AND MAGNETIZATION (CHIARA TARANTINI) AND MICROSTRUCTURAL CHARACTERIZATION (GRADUATE STUDENT CHRIS SEGAL)

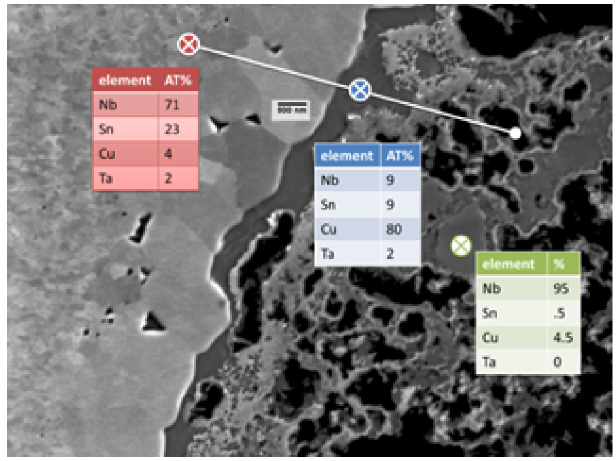

Figure 15 FESEM-BSE image of atypical filament showing SG, LG, membrane and core with superimposed the chemical analysis performed in different points.

In order to investigated the formation of the A15 phase with different morphologies in PIT wires we studied the properties of samples heat treated at low temperature. We found that up to 600 °C there is no large grain A15, but they forms and they have a clearly distinct T_c at 620 °C. This result might be helpful to find a heat treatment that reduces the large grain formation.

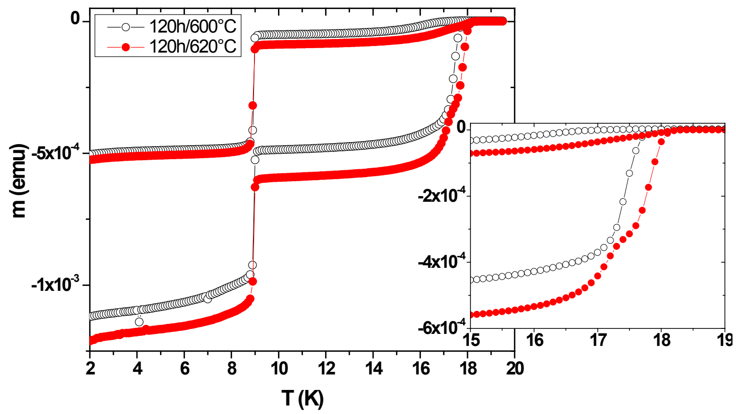

Figure 16 Magnetization measurements of for the two 1 mm-PIT samples heat treated at low temperature.

For this experiment we used Bruker 1 mm-PIT samples with 192 Nb7.5wt.%Ta tube filaments and we considered the 120h/600°C and 120h/620°C heat treatments. Specific heat measurements indicated that a small amount of A15 phase forms at these temperatures: in fact Nb constitutes about ~47% and ~81-82% of the superconducting material for the 120h/620°C and 120h/600°C samples, respectively, and there are also indications of a significant presence of low-T_c phases (below 9 K). We found that T_c onset of the A15 phase is 18.3 and 18 K for the 120h/620°C and 120h/600°C samples, respectively. Because of the low fraction of superconducting materials in the samples, the data quality is preventing T_c-distribution analysis.

In this case, magnetization measurements can provide a more valuable characterization of the superconducting properties. In fact, the curves in Figure 16 reveal that 120h/600°C sample has a single A15 transition with an onset of 18.0 K, whereas 120h/620°C sample has a clear double transition for the A15 phase with an onset of about 18.3 K. These T_c onset values match with those determined by specific heat. These single and double transitions are consistent with what revealed by SEM characterization (Figure 17). In fact at 600°C (left and center images) there is no large grain layer and only few potential nucleation points are visible between the very thin small grain layer and the Nb_6Sn_5 layer: this means that the single transition detected by magnetization has to be ascribed to the small grain A15. At 620°C both the small and large grains are visible suggesting that the highest transition at 18.3 K is due to the large grain formation.

PIT-0.85 MM: SUPERCONDUCTING PROPERTIES BY SPECIFIC HEAT (CHIARA TARANTINI)

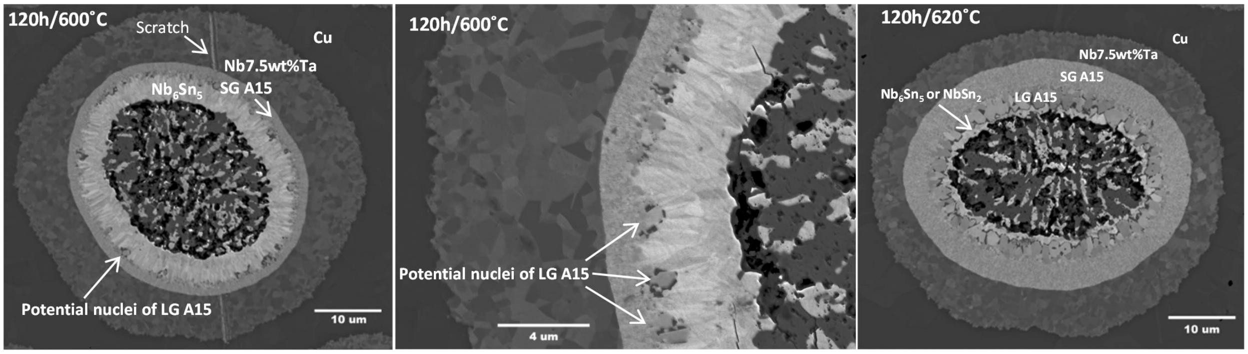

Figure 17 SEM images of the two 1 mm-PIT samples heat treated at 120h/600°C (left and center) and at 120h/620°C (right), showing the presence of a small grain (SG) layer and no large grains (LG) in the first case, whereas at 620°C both SG and LG layers are visible.

In order to optimized the properties of the smaller filament size 0.85 mm Bruker PIT with 192 Nb7.5wt.%Ta tube filaments, we characterized strands after heat treatments in the 630-670 °C range. We found that, despite the different amount of A15 that forms, there is a relatively small difference in the phase homogeneity. However the 0.85 mm strands result having a more homogeneous A15 phase that the nearly optimized 1 mm-PIT.

Several samples from the same billet were heat treated at CERN between 630 and 670 °C for times varying from 50 to 200 hours. Here we summary the results obtained for three of them: 100h/630°C, 200h/630°C and 100h/670°C.

Table 4 Properties of the 0.85 mm-PIT strands compared to nearly optimized 1 mm-PIT ones.

Wire	Residual Nb	RRR	T_c onset
630˚C/100h - 0.85 mm	**34.9 %**	**288**	**18.4 K**
630˚C/200h - 0.85 mm	**23.2%**	**163**	**18.4 K**
670˚C/100h - 0.85 mm	**19.4%**	**61**	**18.5 K**
625˚C/280h-1 mm	20.7%	>150	18.6 K
620˚C/120h+ 640˚C/120h -1 mm	17.7%	>150	18.6 K

Figure 18 shows that both 200h/630°C and 100h/670°C produce more A15 that 100h/630°C. The first two samples leave 23.2 and 19.4% of unreacted Nb, whereas 100h/630°C has almost 35% of it. In the nearly optimized 1 mm strands the residual Nb was 17.7 and 20.7% (all data are summarized in Table 4). The interest in these values is due to the effectiveness of the Nb barrier in preserving the RRR of the Cu stabilizer. In fact in the 1 mm strand 17.7% of residual Nb is enough in maintaining RRR above 150, whereas in the 0.85 mm strand 19.4% is not sufficient and RRR becomes inacceptable. A slightly smaller T_c onset is also observed in the 0.85 mm strand: however, considering that the highest T_c phase in the 1 mm strand was attributed mostly to disconnected A15 grains in the core, the lower onset might indicate a better use of the available Sn.

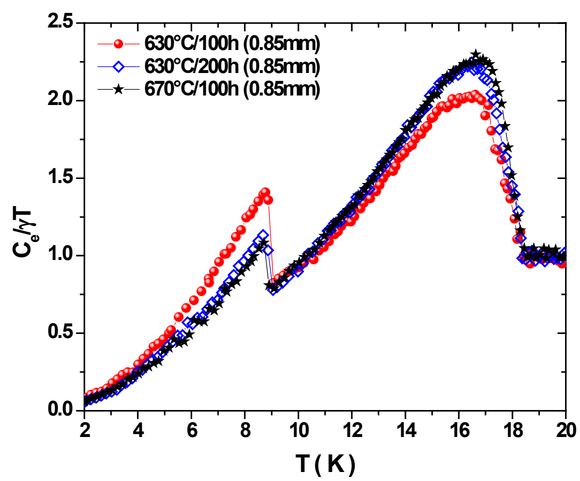

Figure 18 Normalized electronic specific heat for the three 0.85 mm-PIT samples after different heat treatment.

From the T_c-distribution analysis we observe also in this case that the F_{A15} curves (Figure 19) start increasing at 5-6 K suggesting that this is intrinsic of the Ta doping independently on strand designs (RRP or PIT) or heat treatment. The 670 °C has a smoother transition in the high temperature region (above 17 K) but in the intermediate temperature range the three heat treatments for the 0.85 mm-PIT produce similar results. In the same plot (Figure 19) the curve for the nearly optimized 1 mm-strands are also reported for comparison. We found a visible difference in the 10-16 K range: the 1 mm strands have in fact a larger amount of A15 phase in this region indicating that they are slightly less homogeneous.

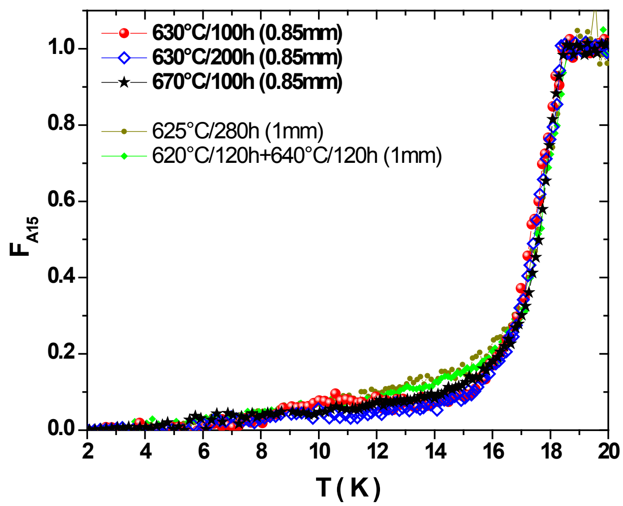

Figure 19 F_{A15}, integral of the A15 T_c-distribution for the three 0.85 mm-PIT samples after different heat treatment. For comparison also the curve for the 1 mm-PIT samples are shown.

III-1H Fundamental Studies Using Bulk Nb_3Sn (Graduate Jian Zhou and Post-Doc Younjung Jo)

The important superconductor Nb_3Sn still presents anomalies and uncertainties, even 52 years after its discovery as the first high field superconductor. In particular, the superconducting mechanism and its sensitivity to structural disorder remain unclear. The important influence of multiple gaps in the superconductivity of MgB_2 and Fe-based compounds, especially because of the possibility that manipulation of a second gap gives can significantly raise the upper critical field H_{c2}, has refocused attention on Nb_3Sn because anomalies in both specific heat and point contact tunneling studies have led to the proposal that Nb_3Sn is also a two-gap superconductor. Here we search for evidence of the second gap in a careful study of the influence of the homogenization temperature on the sample uniformity. We show that it is very difficult to fabricate samples that are both homogeneous and stoichiometric. We find so-called "second-gap" anomalies disappear only after high temperature and long-term annealing. Such a well-annealed sample shows only a strong, electron-phonon-coupled, single-gap behavior. In contrast, samples reacted and annealed at lower temperatures, as in the earlier two-gap studies, show small chemical composition variations of the A15 phase. We propose that the second gap sightings are actually due to variation of T_c within very difficult-to-fully-homogenize samples. A curiosity of this phase is that almost any mixture of Nb and Sn tries to form a stoichiometric A15 composition but the residue of course must always contain off-stoichiometric and other phases when the Nb:Sn ratio departs from the true 3:1 stoichiometry. This work has recently been accepted for publication in APL Materials.

III-2. High T_c Cuprates: Studies of REBCO Coated Conductors and round wire Bi-2212

III-2A Bi-2212: development of single grain boundary extraction technique by using focused ion beam (Fumitake Kametani)

Recent breakthrough in high J_c Bi-2212 round wires has imposed the one big question: Why can Bi-2212 develop high J_c in a round wire form in which the grain boundary (GB) misorientations are far greater than 3-5°, the threshold that previous bi-crystal experiments strongly suggested? Accessing current transport properties at the naturally formed grain boundaries (GBs) is crucial to nail down whether the GBs in Bi-2212 round wires are superior to those in other HTS such as Bi2223 or REBCO. However, because of 3-dimensional, complicated GB geometries and the randomness of the grain orientations, it is very difficult to extract an individual GB from Bi-2212 filaments for carrying out the transport measurements.

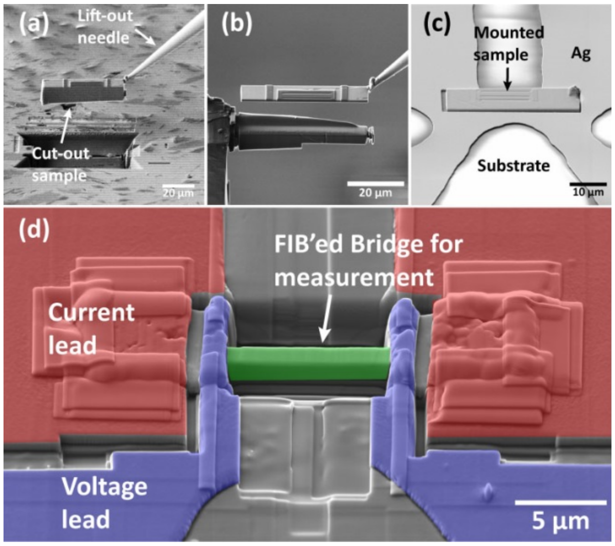

Figure 20. Brief illustration of FIB extraction and sculpting to forms a sample for electromagnetic characterization. (a) Cutting and lift-out. (b) Sculpting to desired shape. (c) Mounting on the Ag-patterned substrate. (d) Sculpture and deposition of metal contacts by GIS. The final bridge width is ~1 µm (the metal contacts and FIBed bridge have been colored to enhance clarity).

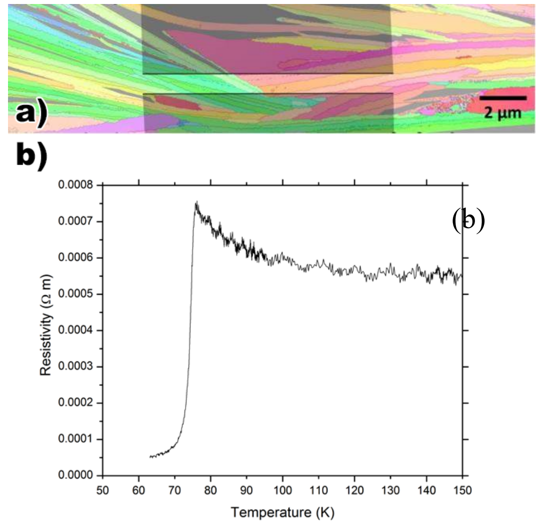

Figure 21. (a) Inverse pole figure map of the bridge of figure 3d. The grain structure derived from EBSD. (b) Temperature dependence of resistivity of grain-colony boundary between greenish and pinkish colonies in (a).

Under the support from HEP, we started to develop the special technique to isolate, extract and measure such 3-dimensional, complex random GBs from polycrystalline samples by utilizing the focused ion beam (FIB). Figure 20 illustrates the procedure of this FIB-extraction technique. After locating the area of interest by electron backscatter diffraction (EBSD), we used the FIB to trench a small piece of it. Then the sample piece is extracted with the OmniProbe lift-out tool and GIS (Figure 20a). The OmniProbe consists of a thin needle with motor drives capable of several axis movements. The extracted piece is then temporarily mounted on a support block at a defined pre-tilt so that the sample can then be flexibly sculpted to the desired shape. As shown in figure 1b, the bottom part of FIB'bed piece was trimmed so as to extract a ~1 µm lamella from the top surface of the sample for transport measurements. The sculpted piece is then lifted out again by the OmniProbe and re-mounted on an Ag-patterned, insulating (e.g. sapphire) substrate (Figure 20c). Once the FIB'bed sample is placed in the substrate slot in proximity to its Ag contact pads, it can be electrically connected to the Ag pattern by bridging the gap with locally deposited Pt using the GIS system. The sample piece is tailored to its final shape after these electrical contacts are made. Figure 20d represents a prototype Bi-2212 sample for which a straight bridge 1 µm wide and ~10 µm long was made. In this case, the grain and GB structure made visible by the prior EBSD was used to define the regions studied by a transport measurement (Figure 21). Our first attempt to measure the FIB-sculptured sample was successful, showing the signature of c-axis transport across the colony boundary in the Bi-2212 filament.

The development of this FIB-sculpture technique is still underway, but it appears very promising to address the local current transport properties at the naturally formed GBs in the melt-processed Bi-2212 round wires.

III-3. Support Of The HEP Community

We continued to provide direct scientific support to the HEP community through continued collaborations with the National Laboratory magnet programs like the Conductor Development Program (CDP) that underpins LARP (Large Accelerator Research Program) and MAP (Muon Accelerator Program) and ongoing broader collaborations of BSCCo (Bi-2212 Strand and Cable Collaboration) with groups at BNL, FNAL, LBNL and the NHMFL that grew out of the just ended VHFSMC (Very High Field Superconducting Magnet Collaboration). These collaborations and our new activities with CERN became central to the work already described above.

III-4. Training

We have continued to provide forefront training to undergraduates, graduates and post-doctorals, maintaining our stream of highly effective and leading personnel to the HEP and the Applied Superconductivity communities (see below). We also actively participated in the NSF sponsored Research Experience for Teachers and Research Experience for Undergraduates programs at NHMFL as well as a high school intern. We have also actively used our undergraduate programs to bring women and minorities into our research environment.

Figure 22. Recent young scientist awards: Fumitake Kametani receives the ICMC 2014 Award for Excellence at the International Cryogenic Materials Conference, U. of Twente, Enschede NL in July 2014, and at the 2014 Applied Superconductivity Conference Christopher Segal wins the Best Student Paper (Materials), Maxime Matras wins The Alexander Shikov Award for the Best Student Paper in Materials on Design and Manufacturing of LTS and HTS Conductors and Carlos Sanabria wins the 2nd place prize for Best Student Paper (Large Scale). Not shown is Chiara Tarantini winning the 2014 Lee Osheroff Richardson North American Science Prize.

One student Pei Li gained his PhD in early 2013 but he has accepted a postdoctoral position with Tengming Shen at Fermilab to work in the HTS conductor and magnet program there.

The excellence of our training has been acknowledged by the recent prizes to all our current graduate students on this project as well as former post-doc Fumitake Kametani (see caption of Figure 22 for details).

Undergraduates

We have a long and successful history of training undergraduates in laboratory research; many of our students have gone on to work in HEP laboratories or related industries. Typically ~8 students are funded are partially funded by this grant.

III-5. Outreach

We continued to co-organize the Low Temperature/High Field Superconductor Workshop (LTSW/HFSW) with LBNL. Starting out in 1983 as an annual program review for the new HEP sponsored program at Applied Superconductivity Center, the meeting has evolved into a remarkably successful meeting of the users, fabricators and understanders of conductors, and it now called the Low Temperature/High Field

Superconductor Workshop. The meetings typically attracted ~90 participants from the HEP community across industry, university and national lab programs. We also continued to provide on-line resources such as the widely trusted and used master critical current density plot. We also remained active in the broader community through our memberships of various workshop and international conference committees (e.g. MT-23, ASC'14, CCA, EUCAS, IEEE-CSC, ISS, M^2S, ICMC).

IV. PUBLICATIONS OVER THE REPORTING PERIOD

a) *Papers which exclusively acknowledge HEP support*

None: All the work in our center includes at least partial support from the State of Florida (75% salary support for PI Peter J. Lee and 100% salary support for Chiara Tarantini) and many of our studies greatly benefit from the NSF funded facilities at NHMFL under NSF/DMR-0654118.

b) *Papers which acknowledge HEP and other agency support - Indicate briefly the role of each acknowledged agency in supporting the research described in the publication.*

See note above regarding global support from the State of Florida and facility support by NSF.

1. "Examination of the tradeoff between intrinsic and extrinsic properties in the optimization of a modern internal tin Nb_3Sn conductor",C. Tarantini, P. J. Lee, N. Craig, A. Ghosh and D. C. Larbalestier, Supercon. Sci and Techn. 27, 065013 (2014).
   http://dx.doi.org/10.1088/0953-2048/27/6/065013
   Funded by HEP with additional salary support from the State of Florida.

2. "Evidence that the upper critical field of Nb_3Sn is independent of whether it is cubic or tetragonal," J. Zhou, Y. Jo, Z-H Sung, H. Zhou, P. J. Lee and D. C. Larbalestier, Appl. Phys. Lett., 99, 122507 (2011).
   http://dx.doi.org/10.1063/1.364305
   Funded by this award and DEFG02-07ER41451, high magnetic field measurements were supported by NSF/DMR-0084173 and by the State of Florida, Younjung Jo was supported by the National Research Foundation of Korea (Contracts NRF 2010-6377 and 2010-20057).

3. "Observation of the Microstructure of Grain Boundary Oxides in Superconducting RF-Quality Niobium With High-Resolution TEM (Transmission Electron Microscope)," Z.-H. Sung, P. J. Lee, and D. C. Larbalestier, IEEE Transactions on Applied Superconductivity, vol. 24, no. 1, pp. 68–73, Feb. 2014.
   http://dx.doi.org/10.1109/TASC.2013.2287050
   This work was supported in part by the U.S. DOE under Grant DE-FG02-05ER41392 and by the FNAL PO 570362, and by the State of Florida. Some funding from this award was provided to investigate new techniques for grain boundary sectioning and imaging of LTS superconductors.

4. Accepted for publication:
   "Specific heat of Nb_3Sn: the case for a single gap," Y. J. Jo, Jian Zhou, Zu Hawn Sung, Peter J. Lee, and D. C. Larbalestier, Applied Physics Letters: Materials, September 2014.
   This work was supported by the NRF (No. 2013R1A1A2063904), BK21Plus project and by this award and the State of Florida.

V. PERSONNEL, GRADUATE STUDENTS, POST-DOCS, VISITORS, TECHNICIANS SUPPORTED BY THIS GRANT

FACULTY/RESEARCH FACULTY

Griffin,Van 1.0 FTE/1 year Other Supp.: Other DOE, NSF, FNAL (DOE flow-thr.), private funds.
Measurements and training students and post-docs in measuring physical property measurements of HEP strands.

Hellstrom,Eric 0.14 FTE/1.75 mo Other Supp.: Other DOE, NSF, FNAL (DOE flow-thr.), State-FL.
2212 relevant for HEP (OP Process)

Jiang,Jianyi .25 FTE/3 mo Other Supp.: Other DOE, NSF, FNAL (DOE flow-thr.).
2212 relevant for HEP (OP Process)

Kametani,Fumitake .33 FTE/4 mo Other Supp.: Other DOE, NSF, FNAL (DOE flow-thr.).
Advance nanofabrication and analysis techniques to test HEP relevant conductors.

Larbalestier,David 0.14 FTE/1.75 mo Other Supp.: Other DOE, NSF, FNAL (DOE flow-thr.), private, State-FL.
Project guidance.

Lee,Peter .21 FTE/2.75 mo Other Supp.: Other DOE, private, State-FL.
Project guidance and quantitative digital microscopy techniques.

Polyanskii,Anatolii 1.25 FTE/ 15 mo Other Supp.: Other DOE, NSF, FNAL (DOE flow-thr.).
Magneto Optical imaging.

Starch,William .25 FTE/3 mo Other Supp.: Other DOE, FNAL (DOE flow-thr.), private, State-FL.
Fabrication and metallographic characterization of training for students and post-docs in those techniques for HEP strands.

Tarantini, Chiara Fully supported for this work by the State of Florida. Specific heat measurements and advanced analysis and student guidance.

GRADUATE STUDENTS

Assume 50% time = 12 months

Brown,Michael 1.75 FTE or 20 mo Other Supp.: Other DOE, private funds.
Additional support was from DOE-OFES (10%) for bulk Nb_3Sn specific to fusion application (low Sn, high Cu) that has being phased out.

Chen,Peng .25 FTE or 3 mo Other Supp.: Other DOE, NSF, FNAL (DOE flow-thr.).

Li,Pei .25 FTE or 3 mo Other Supp.: Other DOE, NSF
Graduated, now at FNAL).

Matras,Maxime .25 FTE or 3 mo Other Supp.: Other DOE, NSF, FNAL (DOE flow-thr.).
2212 relevant for HEP (OP Process).

Sanabria,Carlos .70 FTE or 8.5 mo Other Supp.: Other DOE, private funds.
Training support in Nb_3Sn microscopy to other grads. Primary support was for ITER TF (ITER Organization), ITER CS (US-ITER), other fusion strand microscopy DOE-OFES. But now HEP.

Segal,Christopher 1.82 or 22 mo Other Supp.: Other DOE, private funds.
Additional support from CERN for analysis of CERN HT'ed strand enhances our ability to study the latest generation of HEP Nb_3Sn strand from Europe.

Xu,Aixia .16 FTE or 2 mo Other Supp. from NSF, FNAL (DOE flow-thr.), ORNL (DOE flow-thr.).
REBCO stodies for HEP application: Graduated, is now at TcSUH.

Zhou,Jian .32 FTE or 4 mo Other Supp.: Other DOE-Fusion support for fusion relevant bulk.
Fundamental studies of bulk Nb_3Sn:Graduated, now at Cummins Technology Center

POST-DOCS

Craig,Natanette C 1.0 FTE or 1 year Other Supp.: Other DOE, NSF, FNAL (DOE flow-thr.), private funds, State-FL

Sung,ZuHawn 1.08 or 13 mo Other Supp.: Other DOE, FNAL (DOE flow-thr.), private funds, Auxillary monies

VISITING FACULTIES

Sung,ZuHawn .45 FTE or 4.5 mo Other Supp.: Other DOE

High resolution analytical microscopy of HEP Nb_3Sn) Other support FNAL for SRF studies of Nb coupons supplied by FNAL, SupraMagnetics of microscopy of novel PIT Nb_3Sn.

Alexander Otto 0.5 FTE

Alternative 2212 powder.

VI. REFERENCES

1. C. D. Hawes, P. J. Lee, and D. C. Larbalestier, "Measurements of the microstructural, microchemical and transition temperature gradients of A15 layers in a high-performance Nb_3Sn powder-in-tube superconducting strand," Superconductor Science and Technology, vol. 19, no. 3, pp. S27–S37, Mar. 2006. http://dx.doi.org/10.1088/0953-2048/19/3/004
2. M. Cantoni, C. Scheuerlein, P.-Y. Pfirter, F. de Borman, J. Rossen, G. Arnau, L. Oberli, and P. Lee, "Sn concentration gradients in Powder-in-Tube superconductors," Journal of Physics: Conference Series, vol. 234, no. 2, p. 022005, Jun. 2010. http://dx.doi.org/10.1088/1742-6596/234/2/022005
3. I. Pong, L.-R. Oberli, and L. Bottura, "Cu diffusion in Nb_3Sn internal tin superconductors during heat treatment," Superconductor Science and Technology, vol. 26, no. 10, p. 105002, Oct. 2013. http://dx.doi.org/10.1088/0953-2048/26/10/105002
4. A. Devred, I. Backbier, D. Bessette, G. Bevillard, M. Gardner, C. Jong, F. Lillaz, N. Mitchell, G. Romano, and A. Vostner, "Challenges and status of ITER conductor production," Superconductor Science and Technology, vol. 27, no. 4, p. 044001, Apr. 2014. http://dx.doi.org/10.1088/0953-2048/27/4/044001
5. C. Tarantini, P.J. Lee, N. Craig, A. Ghosh and D.C. Larbalestier, "Examination of the tradeoff between intrinsic and extrinsic properties in the optimization of a modern internal tin Nb_3Sn conductor", Supercond. Sci. Technol.27, 065013 (2014). http://dx.doi.org/10.1088/0953-2048/27/6/065013